

**DIRECTED C-O ACTIVATION OF NITRILE FUNCTIONALIZED
ALKYL ETHERS: C-C CROSS COUPLING USING REDOX-
ACTIVE COBALT CATALYSTS**

A Thesis
Presented to
The Academic Faculty

by

Quinton Bruch

In Partial Fulfillment
of the Requirements for the Degree
Bachelors of Science with the Research Option in the
School of Chemistry & Biochemistry

Georgia Institute of Technology
May 2016

COPYRIGHT 2016 BY QUINTON BRUCH

**DIRECTED C-O ACTIVATION OF NITRILE FUNCTIONALIZED
ALKYL ETHERS: C-C CROSS COUPLING USING REDOX-
ACTIVE COBALT CATALYSTS**

Approved by:

Dr. Jake Soper, Advisor, Advisor
School of Chemistry & Biochemistry
Georgia Institute of Technology

Dr. Joseph Sadighi
School of Chemistry & Biochemistry
Georgia Institute of Technology

Date Approved: [Date Approved by Committee]

ACKNOWLEDGEMENTS

I would like to thank Dr. Jake Soper for his guidance over the past three years and the role he has played in shaping my scientific and research abilities and interests. I would also like to thank the past and present members of the group for their time, friendship, mentorship, assistance, and patience as I learned how to do just about everything. To my mentors, in research, academia, and life, I'd like to thank Dr. Jillian Dempsey, Dr. Joseph Sadighi, and Dr. Loren Williams for their time, kindness, and mentorship. To the friends and family that have supported me throughout my undergraduate career, especially my parents Stephanie and Gerald Bruch, Ashlyn Norris, Amaan Kazerouni, and 2nd Floor Gunn; thank you. Finally, I would like to acknowledge the support for my time here from both the President's Undergraduate Research Award (PURA) and the President's Scholarship Program.

TABLE OF CONTENTS

	Page
ACKNOWLEDGEMENTS	iv
LIST OF TABLES	vii
LIST OF FIGURES	viii
LIST OF SYMBOLS AND ABBREVIATIONS	ix
SUMMARY	xi
<u>CHAPTER</u>	
1 Introduction	1
General Mechanisms of Cross Coupling	3
Palladium Catalyzed Cross Couplings	3
Base-Metal-Catalyzed Cross Couplings	4
Base Metal C-O Activation for C-C Bond Formation	6
Base Metal Ether C-O Activations	7
Redox-Active Ligands	8
<i>N</i> -Heterocyclic Carbenes	10
2 Methods and Methodology	12
General Materials	12
Instrumentation	12
General Methodology	13
Synthesis of Cobalt Catalysts	13
Experimental Procedures	14
3 Results	16
Synthesis and Characterization of $\text{Co}^{\text{II}}((\text{tBuPhO})_2\text{PhNHC})\text{MeCN}$	16

Ether C-O Bond Activation and Cross Coupling with Aryl Magnesium Halides	17
Optimization of Reaction Conditions	18
Optimization of Reaction Concentrations and Catalyst Loading	20
Investigations into Substrate Tolerance	22
Variation of C-O Substrates	22
Variation of Organometallic Substrates	27
Kumada Coupling	30
Investigations into Catalytic Intermediate Species	32
4 Discussion	34
Investigating Reaction Conditions of C-O Activation	34
Understanding Directing Group's Role in C-O Activation	37
Determining the Reaction Pathway of C-O Cleavage and C-C Formation	41
5 Conclusions	46
6 Future Works	48
REFERENCES	50

LIST OF TABLES

	Page
Table 1.1: Summary of palladium cross couplings.	3
Table 3.1: Impact of additives on C-C bond formation.	20
Table 3.2: Impact of varying butoxy-nitrile carbon linkers and alkoxy chain length on coupling of ether nitriles with phenylmagnesium bromide using 5% CoSNHC.	24
Table 3.3: Impact of rigidity between alkoxy and nitrile chain, accounting for a variety of alkoxy chain lengths.	25
Table 3.4: Ability of other functional groups to drive for C-O activation, accounting for acidic proton quenching of Grignards.	26
Table 3.5: Coupling of unactivated and undirected sp^3 C-O bonds with phenylmagnesium bromide at 5% CoSNHC. Ether reagents are in large excess.	27
Table 3.6: Coupling of 3-butoxypropionitrile with various organometallics at 5% CoSNHC at room temperature for 24 hours.	28
Table 3.7: Effect of various functional groups on the aryl ring of Grignards for coupling with 3-butoxypropionitrile.	30
Table 3.8: Kumada coupling of halogenic alkyl nitriles with PhMgBr with 2.5% CoSNHC under heated conditions for 1 hour.	31

LIST OF FIGURES

	Page
Figure 1.1: Pd-catalyzed Kumada coupling mechanism.	4
Figure 1.2: Three radical pathways for Kumada coupling of an Fe(II) complex.	5
Figure 1.3: Redox-neutral activation of C-O aryl ethers using a nickel salt.	7
Figure 1.4: Addition of methylene chloride to [Co(ap) ²].	9
Figure 1.5: Bis-phenolate NHC varying from saturated to benzylic backbone.	11
Figure 3.1: Structure of CoSNHC (left) and CoPhNHC (right).	16
Figure 3.2: Cyclic voltammogram of CoSNHC (red) compared to CoPhNHC (gold) in MeCN	17
Figure 3.3: Generic reaction scheme for C-O cross coupling reaction.	17
Figure 3.4: Varying Grignard equivalents versus ether nitrile with linear region (orange) and non-linear region (blue).	19
Figure 3.5: Yields at various catalyst loadings of CoSNHC at fixed concentrations of catalyst (blue) and fixed concentrations of reagent (orange).	21
Figure 3.6: Linearization of yields at various catalyst loadings of CoSNHC by measuring TON as a function of catalyst loading.	21
Figure 3.7: Proposed interactions of CoSNHC with reagents	32
Figure 3.8: Bleaching of CoSNHC spectra with subsequent additions of Grignard.	33
Figure 3.9: Reformation of CoSNHC from 2a in a cuvette under sealed N ₂ atmosphere.	33
Figure 4.1: Generic reaction scheme for C-O cross coupling reaction.	35
Figure 4.2: Potential binding modes of 3-butoxypropionitrile to CoSNHC to form 2b .	37
Figure 4.3: Redox-neutral pathway of C-O activation via CoSNHC. The ligand arms have been excluded for simplicity and size.	42
Figure 4.4: Redox-active pathway of C-O activation via CoSNHC.	43

LIST OF SYMBOLS AND ABBREVIATIONS

Ar	Aryl
ATR	Attenuated Total Reflection
CV	Cyclic Voltammetry
CDCl ₃	Chloroform- <i>d</i>
°C	Degrees Celsius
Fc	Ferrocene
FTIR	Fourier Transform Infrared
GC-MS	Gas Chromatography-Mass Spectrometry
PF ₆	Hexafluorophosphate
Hexyl-MgBr	Hexylmagnesium bromide
LiHMDS	Lithium hexamethyldisilylamide
OMs	Methanesulfonate (mesylate)
MeOH	Methanol
mL	milliliter
mM	millimolar
μL	microliter
ε	Molar Absorptivity
nBu	<i>n</i> -butyl
NHC	<i>N</i> -Heterocyclic Carbene
NMR	Nuclear Magnetic Resonance
ppm	Parts per million
PhLi	Phenyllithium

PhMgBr	Phenylmagnesium bromide
PhZnBr	Phenylzinc bromide
R.T.	Room Temperature
NaOMe	Sodium Methoxide
<i>t</i> -BuLi	<i>tert</i> -Butyl lithium
THF	Tetrahydrofuran
TMS	Tetramethylsilane
OTs	<i>p</i> -Toluenesulfonate (tosylate)
OTf	Trifluoromethanesulfonate (triflate)
V	Volts

SUMMARY

The utility of palladium in cross coupling is driving efforts to find alternatives based on inexpensive, abundant first-row transition metals. Beyond mimicking Pd, base metal catalysts can access entirely new reactions unknown to precious metals. A recently discovered coupling of ether nitriles and aryl Grignards was herein optimized with Co^{II} bis(phenol)-substituted *N*-heterocyclic carbene complexes. Reactivity was explored with a variety of directed, activated, and both unactivated and undirected ether reagents. Coupling seemed specific to nitrile directing groups, with a 3-carbon linker being optimal, with optimized yields of >70% at 5 mol% catalyst loading at 70 °C. A variety of organometallic coupling partners were also explored, with aryl- and alkyl-lithium, Grignard, and organozinc reagents.

The activation and functionalization of C-O bonds is of special importance, as it can play a powerful role in late-stage fine chemical synthesis. This system is of interest, as it activates sp³ C-O bonds, a rare process, and constitutes the first non-aryl containing ether C-O activation for C-C bond formation. Mechanistic investigations of this system determined it followed a redox-active pathway instead of an acid-base activation. Tests using Kumada reagents suggest that the redox-active pathway that C-O reagents pass through is fundamentally different.

CHAPTER 1

INTRODUCTION

The utilization of base metals for cross coupling reactions is of increasing importance to industrial and pharmaceutical chemistry as it offers sustainable and safe synthetic routes as compared to state-of-the-art palladium.¹ Base metal cross coupling catalysts have been known since at least the 1970s, but have only recently seen a resurgence of interest.²⁻⁵ This is because first-row transition metals such as cobalt, iron, nickel, and manganese are significantly cheaper and generally less toxic than palladium, and offer opportunities to both mimic Pd catalysis and access novel reactions.²⁻⁵ Even with the wealth of methodology for C-C cross couplings using Pd, progress made in first-row metal coupling catalysts might pave the way for industrial processes that can phase out palladium in areas including fine chemicals synthesis and pharmaceuticals.²

The primary challenge in directly eliciting Pd-like catalysis at a first-row metal is the consequence of preferred oxidation states between the metals themselves. For example, Pd-catalyzed Suzuki and Negishi couplings proceed through discrete two electron steps, oxidative addition and reductive elimination, accessing Pd⁰/Pd^{II} redox cycles. In contrast, many first-row metals favor single electron oxidation state changes. Naturally occurring Fe and Co are typically dicationic and tricationic salts. To therefore effect two-electron redox cycles on either Fe or Co would require accessing unstable intermediates such as Fe(I), Fe(IV), Co(I), or Co(IV) respectively. Though not unprecedented, these oxidation states are more easily reached with the assistance of redox active ligands.

One strategy to address this discrepancy in oxidation states utilizes cooperative metal-ligand redox chemistry. Unlike many ligands, which are redox inert, redox active ligands are able to mask these oxidation states by storing or removing electrons from the ligand. Redox active ligands have been studied heavily in the past few decades, with most of the focus on understanding the delocalization of the electron density and how that affects both formal and experimental oxidation states. In recent years, redox-active ligands have found applications in stoichiometric bond-making and –breaking reactions and mechanistic studies have elaborated many of the features that enable the base metals to undergo two electron organometallic-type reaction steps.⁶ This fundamental understanding can then be applied to redox-active catalysts.⁶ Ultimately, understanding how base metals enact these steps allows for improved ligand and catalyst design, moving one step closer to industrial viability.

This thesis focuses on understanding the role of a redox active *N*-heterocyclic carbene (NHC) bisamidophenolate ligand in a cobalt catalyzed C-O activation, ultimately leading to C-C bond formation with aryl Grignard reagents. Previous investigations of C-O activations using base metal have predominantly proceeded on nickel, with some repeat reactivity shown on cobalt.⁷ Neither metal has been reported to utilize unactivated sp³ alkyl ethers, with this work being a novel example. Further developments in C-O activation for C-C bond formation are of particular importance, as this would greatly improve chemists' ability to perform late-stage functionalization of molecules, providing access to a variety of current and proposed fine chemicals.

General Mechanisms of Cross Coupling

Since their discovery in the 1970s, palladium couplings have revolutionized synthetic chemistry for their versatility in forming new C-C bonds, culminating in the joint awarding of the 2010 Nobel Prize in Chemistry to Negishi, Heck, and Suzuki. Other couplings such as Stille, Sonogashira, Buchwald-Hartwig amination, and Kumada coupling have since been discovered and their reagents and products are all summarized below in **Table 1.1** where R is generally an alkyl, aryl, or vinyl.

Table 1.1. Summary of palladium cross couplings.

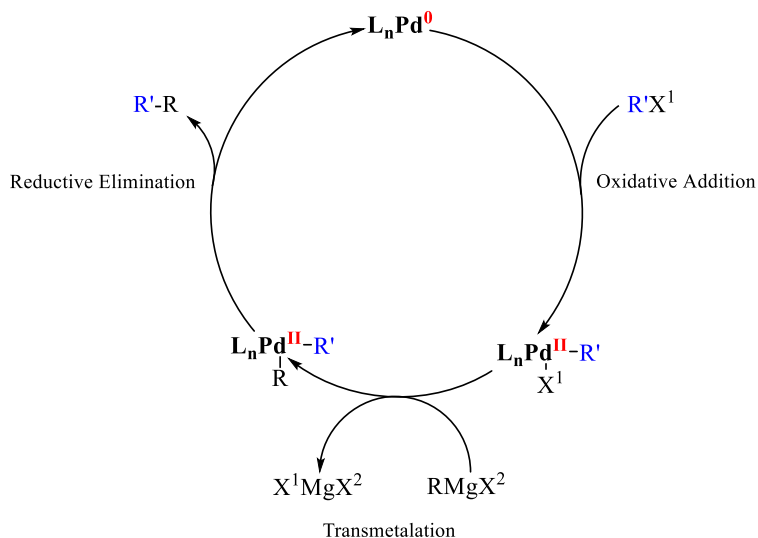
Named Coupling	Reagent	Coupling Partner	Product
Negishi	R-X	R'-Zn-X	R-R'
Heck	R-X	Alkene	R-Alkene
Suzuki	R-X	R'-B(OR) ₂	R-R'
Stille	R-X	R'-Sn(Alkyl) ₃	R-R'
Sonogoshira	Ar-X	Alkyne	Ar-Alkyne
Buchwald-Hartwig	Ar-X	Amine	Ar-Amine
Kumada	R-X	R'-Mg-X	R-R'

Palladium Catalyzed Cross Couplings

The majority of these reactions proceed through the coupling of an organohalide and an organometallic complex, proceeding through qualitatively similar two electron oxidative addition and reductive elimination steps. An example mechanism is shown below in **Figure 1.1** for the Kumada coupling of an organohalide and a Grignard reagent. For Kumada coupling, the palladium catalyst starts at a Pd(0) oxidation state and undergoes a two electron oxidation upon cleavage of the carbon-halogen bond during oxidative addition giving a Pd(II) species bound to both a halogen, X, and an organic fragment, R. The halogen is then exchanged with the organic fragment of a Grignard

reagent during transmetalation to yield a Pd(II) species bound to two distinct organic fragments, R and R'. This species then undergoes a two electron reduction reforming the Pd(0) species and a new C-C bond in the desired product, R-R'. This mechanism is largely preserved in Negishi, Stille, and Sonogashira while the Heck, Suzuki, and Buchwald-Hartwig couplings rely on the addition of base to activate/reform their Pd(0) catalyst. This simplicity of mechanism in many cases is one of the starkest contrasts between palladium and base metal couplings, as it allows for more facile identification of preferred ligand characteristics as well as optimization of the catalytic system.

Figure 1.1. Pd-catalyzed Kumada coupling mechanism.

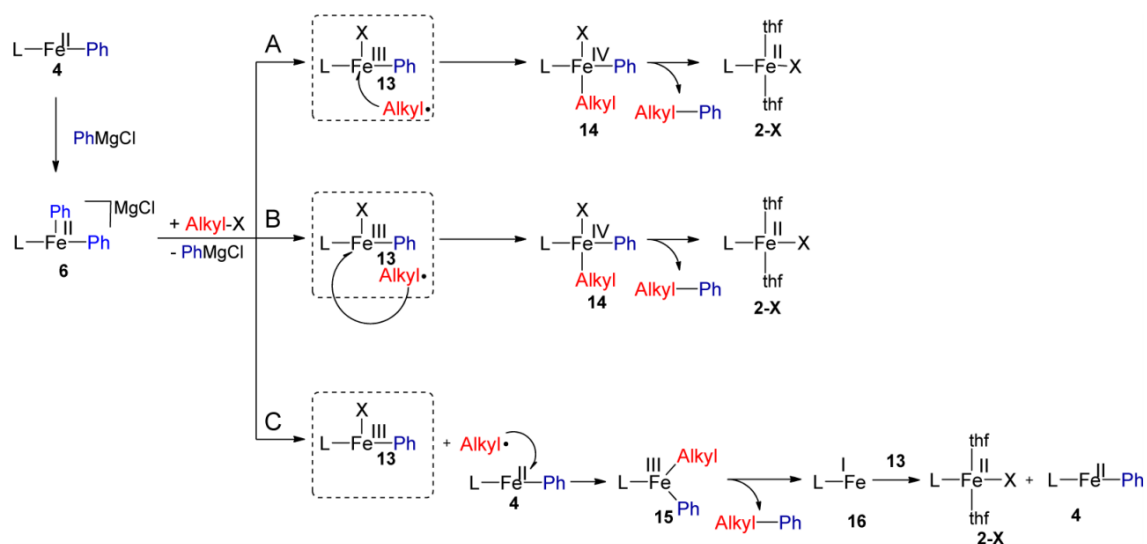


Base-Metal-Catalyzed Cross Couplings

In contrast, the tendency of base metals toward single-electron redox process can introduce a variety of radical path mechanisms or a mixture of radical and traditional steps. The first example shown below in **Figure 1.2** explores Kumada coupling of an Fe(II) complex. Unlike palladium chemistry, this reaction proceeds through a radical intermediate, which was thought to proceed through three potential pathways for product

formation. Of these two pathways, **A** and **B** proceed through subsequent single electron oxidations via radical alkyl attack at iron forming an Fe(IV) species which reductively eliminates back to the initial Fe(II) species.⁸ The remaining **C** pathway features halogen transfer to the iron metal center, with subsequent halogen loss prior to alkyl radical attack, forming an Fe(III) species.⁸ This then reductively eliminates to form the product and an Fe(I) species.⁸ This low-valent species is much more reactive than the starting Fe(II) species, favorably undergoing oxidative addition to form an Fe(III) species that comproportionates with the Fe(I) to form the initial Fe(II) complex and an Fe(II) intermediate.⁸ Ultimately, even after extensive kinetic studies and intermediate isolations, it was not possible to definitively confirm a single pathway, instead only indicating pathway C as the most likely or preferred path.⁸ In comparison to palladium-catalyzed cross coupling, base metal mechanisms have the potential for a variety of novel pathways.

Figure 1.2. Three radical pathways for Kumada coupling of an Fe(II) complex.⁸

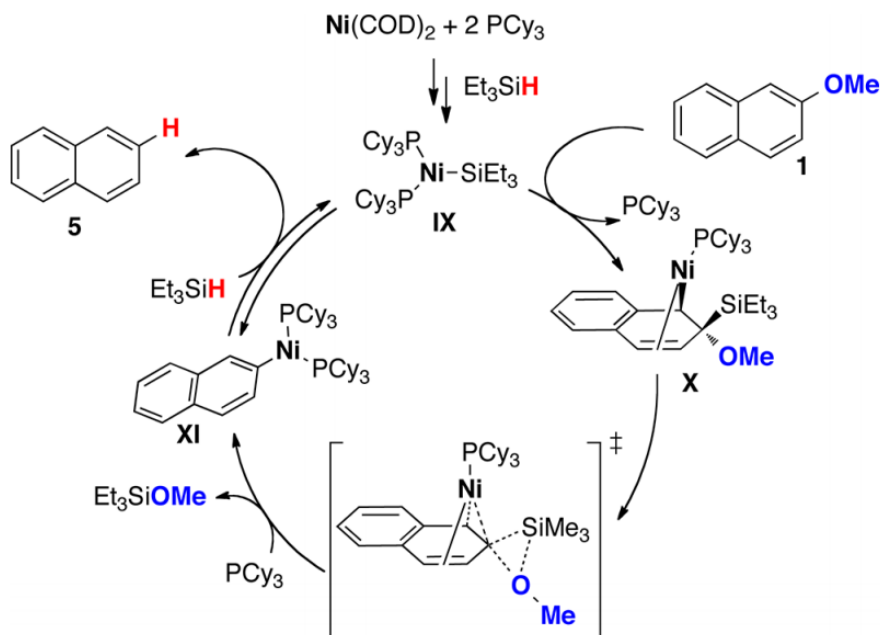


Base Metal C-O Activation for C-C Bond Formation

Activation and selective functionalization of C-O bonds is currently one of the most attractive targets for catalysis.⁷ However, the C-O bond in organic chemistry is relatively inert, making the subsequent functionalization inherently more difficult, and until recently, limited to late and noble transition metals.⁹ These transformations also generally proceed first through transformation of the C-O bond to a more reactive C-Halogen or C-X (X= OTf, OTs, OMs) before C-C bond formation.⁷ However, recent work on nickel, iron, and cobalt has shown their propensity to couple activated C-O bonds using both boronic acids and Grignards as coupling partners.

Of the three, nickel has shown the greatest scope of reactivity with C-O bonds, activating ethers, esters, carboxylates, carbamates, and alkyl and aryl alcohols. The activity of nickel towards activating the C-O bond has been attributed both to the nucleophilicity of the 3d metal, in comparison to palladium and platinum, but also its competence of (0/II) and (I/III) two-electron cycles unlike, iron and cobalt.⁷ However, as discussed in above sections, this does not preclude the occurrence of radical or redox-neutral mechanisms as shown by the mechanism for aryl ether activations below in **Figure 1.3.**¹⁰

Figure 1.3. Redox-neutral activation of C-O aryl ethers using a nickel salt.¹⁰



Though more limited in scope, subsequent C-O activation studies on iron and cobalt have shown similar reactivity to nickel, reacting with sulfonates, esters, carbamates, and naphthyl alcohols, alkenyl carboxylates, and benzylic ethers for either cobalt or iron.^{7,11-14} However, the advent of better ligand design could assist in designing cobalt and iron catalysts more similar to the nickel systems already developed, namely improved nucleophilicity and stability of two electron cycles.

Base Metal Ether C-O Activations

Ether C-O bonds are traditionally viewed as one of the most inert C-O bonds and are readily used in organic synthesis for the protection of alcohols. However, if such bonds could be functionalized, it would open a variety of new synthetic routes to useful industrial and fine chemicals, particularly if the catalysis could proceed with stereospecificity.^{7,15} This is one area where nickel has outshone both precious metals and

other 3d metals, as it has shown the most reactivity with both aryl and alkenyl ethers in coupling reactions; however, further investigations are need on nickel and other metals to further understand the scope of such couplings.^{7,15} Currently the only two coupling partners used have been either Grignards or organoboranes, which are thought to first activate the C-O bond through formation of adducts. Ultimately, this improves the electrophilicity about the C-O bond, improving the nucleophilic attack of the nickel catalyst.^{7,16,17} This also applies to the only case of ether activation, involving iron with no examples of ether C-O activation using cobalt.¹⁸ Therefore this work seeks to explore the role of the cobalt catalyst in C-O activation both mechanistically, and identification of structure-function relationship of the ligand selected. The potential for magnesium-promoted catalysis will also be explored to determine the role of any adduct complexes that may form.

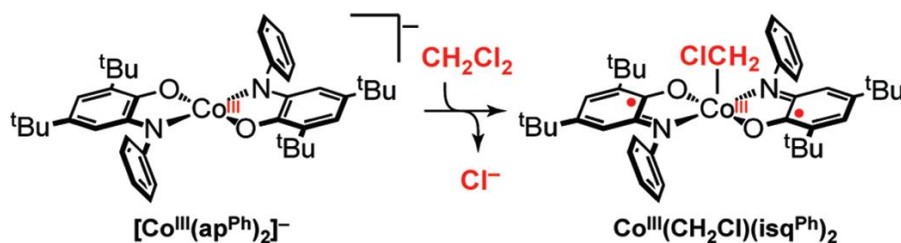
Redox-Active Ligands

The inclusion of redox-active ligands in base metal catalysis has seen widespread adoption for the development of ranging from Kumada-like couplings shown in this work, to hydroboration of alkenes.¹⁹ Redox-active ligands are simply any ligand bound to the metal center that formally accept or supply electrons to the metal center during oxidation or reduction. This process is sometimes called ligand “non-innocence” which complicates the assignment of oxidation state at the metal center, as a redox-active ligand does not necessarily fully donate or accept electrons in discrete integers. Two relevant classes of redox-active ligands to this work are amidophenolates and *N*-heterocyclic carbenes (NHC), both of which have been studied electrochemically to determine the

oxidation state of cobalt versus the ligand during, one and two electron oxidations. They have also previously shown catalysis for C-C bond formation.

Recent work completed by Smith et al. focused heavily on the characterization of cobalt bis(amidophenolate) complexes, extensively studying their ability to stabilize formally Co(III/V) species and their subsequent ability to reductively eliminate C-C or C-Cl bonds.^{20,21} Their work showed that a Co(III) center supported by two amidophenolate ligands are capable of oxidatively adding methylene chloride, while retaining Co(III) at the metal center.²⁰ Instead of forming the unfavorable Co(V), each amidophenolate ligand loses one electron, forming a diradical compound as shown below in **Figure 1.4**. Further investigations of the addition mechanism revealed that it was predicated on the strongly nucleophilic cobalt metal center combined with lower oxidation potentials of the ligand.²⁰

Figure 1.4. Addition of methylene chloride to $[\text{Co}(\text{ap})^2]$.



The analogous ethyl complex was also made and shown to react with arylzinc reagents through Negishi coupling. However, the coupling reaction proceeded with poor yields due to a slow isomerization step necessary for C-C bond formation.²⁰ It was therefore proposed that if the amidophenolate ligands could be tethered in a rigid fashion, it would enforce a preferred geometry ultimately improving catalysis. There are a variety of tethering moieties, including linking the di-*tert*-butylphenoxide arms with pyridines,

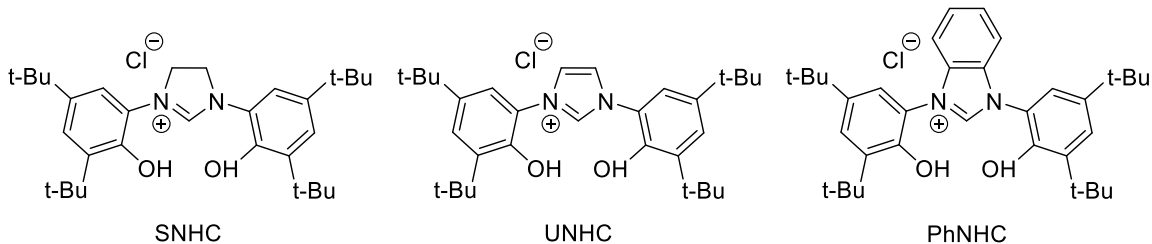
arenes, furans, thiophenes, and *N*-heterocyclic carbenes (NHCs). An NHC and its derivatives were used in this study to explore catalysis.

***N*-Heterocyclic Carbenes**

The employment of an NHC to tether the amidophenolates has resulted in bis-phenolate NHC ligands that have been extensively studied in the laboratory of Dagorne and Bellemin-Laponnaz on a variety of metals spanning the transition metal series.²²⁻²⁴ One of their more recent works explored the ligand's ability to reductively eliminate benzyl fragments to the carbene on Zr(IV), which is generally viewed as electronically inert.²³ This means that the two electrons necessary for C-C bond formation had to be mediated through the ligand, and not the metal center. Therefore, it is plausible to assume that the ligand's ability to move two electrons can assist in oxidative addition and reductive elimination processes on later 3d metals such as cobalt. However, distinct from the zirconium non-innocence shown, cobalt complexes would be able to mediate the transfer of two electrons into and from the ligand assisting in bond breaking and forming steps.

The Dagorne and Bellemin-Laponnaz labs have also explored the structural and electronic features of the bis-phenolate NHC ligands on nickel, palladium, and platinum. They explicitly explored these states using DFT calculations for various molecular orbital occupancy states for varying saturation of the NHC backbone and found that the HOMO was centered on the metal and phenolate regions of the ligand while the LUMO was mainly located on the ancillary solvent ligand.²² The non-metallated ligands are shown below in **Figure 1.5**.

Figure 1.5. Bis-phenolate NHC varying from saturated to benzylic backbone.



Until very recently, one thing lacking from Dagorne and Bellemin-Laponnaz's characterization was experimental evidence for ligand redox non-innocence. This has now been explicitly shown by electrochemical and structural investigations of Co(II) complexes supported by NHC ligands, as shown by Bayless et al.⁶ Bayless et al. found that Co(II) complexes supported by a SNHC ligand undergo three reversible oxidations, and that the formally isolated Co(III) species features a metal-based oxidation while the formally Co(IV) species is actually Co(II) with diradical character on the ligand.⁶

Investigations were expanded to Co(II)UNHC and Co(II)PhNHC compounds to determine whether the change in backbone would shift the oxidation potentials, and desaturation of the backbone played the largest role, resulting in higher oxidation potentials. However, the rigidity of the PhNHC backbone versus the UNHC backbone was shown to have little impact on the electrochemistry of these compounds.

This work employs both Co(II)SNHC and Co(II)PhNHC, seeking to understand if the changes in oxidation potentials will play a meaningful role in C-O activation catalysis. To simplify nomenclature, oxidation states for the cobalt catalyst will be assigned based on the formal oxidation state of the metal, which assumes all ligands are redox innocent. Where relevant in mechanistic studies, ligand-based electrons will be explicitly stated or drawn.

CHAPTER 2

MATERIALS AND METHODOLOGY

General Materials

Unless otherwise noted, all manipulations were performed under an air and moisture-free atmosphere using standard Schlenk line techniques or in an inert atmosphere glove box under purified nitrogen. Solvents for air- and moisture-sensitive manipulations were purchased from Sigma-Aldrich, further dried over activated alumina, and degassed by at least three freeze-pump-thaw (FPT) cycles before being stored under N₂ atmosphere for use. Deuterated solvents were purchased from Cambridge Isotope Laboratories, Inc. All other chemicals were acquired from commercial sources. If the chemical was a liquid, it was degassed using FPT procedures prior use. Catalysts were synthesized following known procedures.

Instrumentation

NMR Experiments

All NMR spectra were acquired on a Varian mercury 300 spectrometer (300.323 MHz for ¹H) at ambient temperature. Chemical shifts are reported in parts per million (ppm) relative to tetramethylsilane (TMS). The solution state magnetic moments of cobalt compounds were determined by the Evans NMR Method.^{25,26}

Cyclic Voltammetry

Cyclic voltammetry (CV) experiments were run under an inert atmosphere using a CH Instruments CHI620C potentiostat in a three-component cell consisting of a platinum disk working electrode, platinum wire auxiliary electrode, and a non-aqueous AgNO₃/Ag

reference electrode. All experiments were performed in CH₃CN with 0.1 M [nBu₄N][PF₆] as the supporting electrolyte with Fc/Fc⁺ used as an internal standard.

Gas Chromatography – Mass Spectrometry

Gas chromatography-mass spectrometry (GC-MS) samples were run using a HP 6890 gas chromatograph with tandem mass spectrometry using a MicroMass AutoSpec M by the Georgia Institute of Technology Bioanalytical Mass spectrometry Facility. GC-MS yields were calculated using a calibration curve constructed using decane as an internal standard.

UV-Vis and FTIR Spectrophotometry

UV-Vis absorption spectra were recorded using a UV-Vis fiber optic probe connected to a UV-Vis spectrometer. IR spectra was obtained using an attenuated total reflection (ATR) diamond plate on a Thermo-Scientific Nicolet 4700 FTIR spectrophotometer.

General Methodology

Synthesis of Cobalt Catalysts

Synthesis of CoSNHC

Synthesis of [Co((tBuPhO)₂NHC)THF]. [tBuPhO)₂NHC]Cl (0.515 g, 1.0 mmol), 0.5 M NaOMe in MeOH (0.600 mL, 3.0 mmol), and MeOH (3mL) combined and stirred to yield a pink solution. CoCl₂ (0.129 g, 1.0 mmol) was then combined with the above solution and stirred until the CoCl₂ had completely dissolved yielding an orange solution.

The resulting solution was then filtered through a fine Buchner funnel and Celite using THF to wash through all orange solids and dried *in vacuo*. The resulting filtrate was taken up in THF (5mL) and passed again through a fine Buchner funnel and Celite using THF to pull the orange solid through and dried *in vacuo* to generate [Co((tBuPhO)₂NHC)THF] (.5462 g, 90% yield). UV-vis (THF) λ_{max} , nm (ϵ , M⁻¹, cm⁻¹): 430 (5.3 * 10³). FTIR (ATR, solid) 2947(m), 2899(m), 2866(m), 1506(m), 1358(m), 869(m), 756(m), 643(m) cm⁻¹.

Synthesis of CoPhNHC

Synthesis of [Co((tBuPhO)₂PhNHC)THF]. [tBuPhO)₂PhNHC]Cl (0.562 g, 1.0 mmol), 0.5 M NaOMe in MeOH (0.600 mL, 3.0 mmol), and MeOH (3mL) combined and stirred to yield a pink solution. CoCl₂ (0.129 g, 1.0 mmol) was then combined with the above solution yielding a green solution and stirred overnight. The resulting orange solution was filtered through a fine Buchner funnel and celite using THF to wash through all orange solids and dried *in vacuo*. The resulting filtrate was taken up in THF (5mL) and passed again through a fine Buchner funnel and celite using THF to pull the orange solid through and dried *in vacuo* to generate [Co((tBuPhO)₂PhNHC)THF] (.5344 g, 81% yield). UV-vis (MeCN) λ_{max} , nm (ϵ , M⁻¹, cm⁻¹): 428 (1.45 * 10³). FTIR (ATR, solid) 2953(l), 2903(m), 2866(m), 2163(m), 1563(m), 1357(l), 860(m), 738(m), 632(m) cm⁻¹.

Experimental Procedures

General Procedure for Cross Coupling

CoSNHC (5.0 mg, 8.2 μ mol) was weighed into a 5mL volumetric flask and dissolved in THF (1 mL) and decane was added (0.005 mL, 25 μ mol) to serve as an internal standard. To this was added 3-butoxypropionitrile (0.228 mL, 165 μ mol) and

PhMgBr (0.826 mL, 165 μ mol) turning the orange solution dark green-brown. The solution was then diluted to 5 mL and was transferred to a 20 mL scintillation vial and capped. After 24 hours the solution was quenched with dried MeOH (1 mL).

General Procedure for Heated Cross Coupling

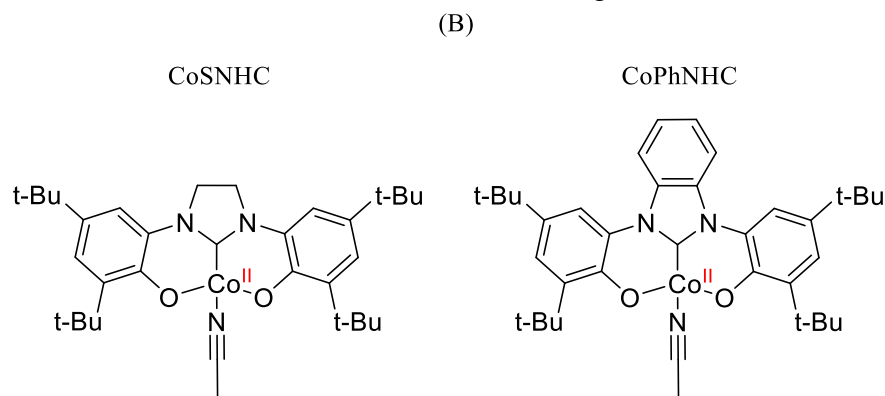
CoSNHC (5.000 mg, 8.2 μ mol) was weighed into a 5 mL volumetric flask and dissolved in THF (1 mL) and decane was added (0.005 mL, 25 μ mol) to serve as an internal standard. To this was added 3-butoxypropionitrile (0.228 mL, 165 μ mol) and PhMgBr (0.826 mL, 165 μ mol) turning the orange solution dark green-brown. The solution was diluted to 5 mL and immediately transferred to a glass bomb, sealed, and heated at the stated temperature for a given amount of time before being quenched with MeOH (1 mL).

RESULTS

Synthesis and Characterization of $\text{Co}^{\text{II}}((\text{tBuPhO})_2\text{PhNHC})\text{MeCN}$

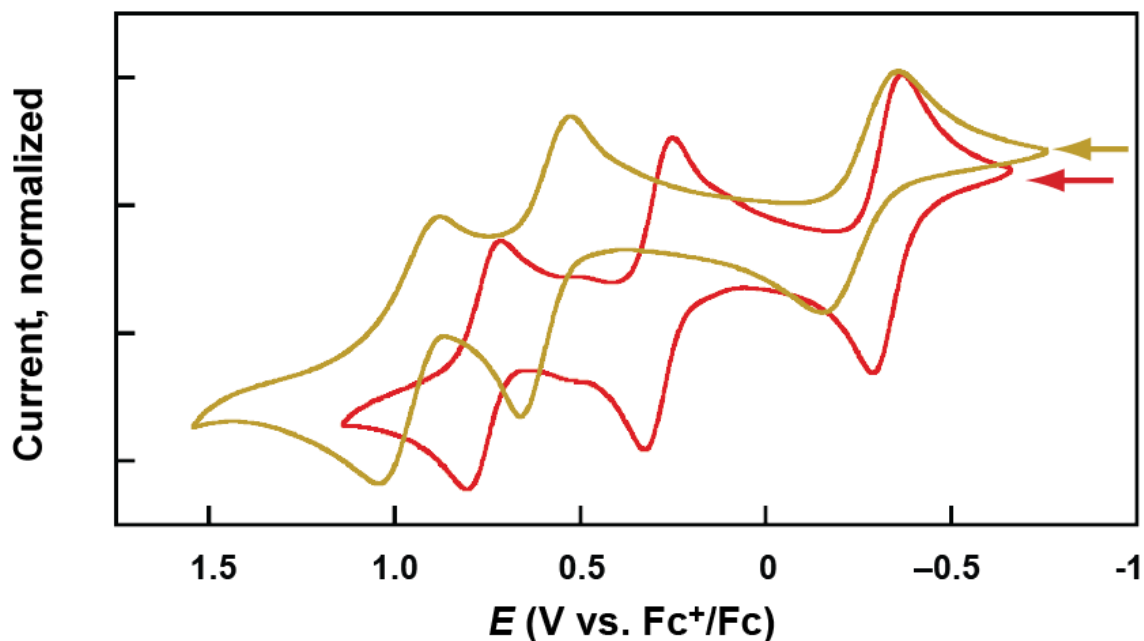
$\text{Co}^{\text{II}}[(\text{tBuPhO})_2\text{PhNHC}]\text{MeCN}$ (CoPhNHC) was synthesized in an inert atmosphere by triply deprotonating 1,3-bis(3,5-di-*tert*-butyl-2-hydroxyphenyl)-1*H*-benzimidazolium chloride using three equivalents of NaOMe in MeOH before stirring overnight with 1 equivalent of CoCl_2 . During this time the solution was observed to convert to an orange color. The solution was dried, taken up in THF, and filtered to yield a clear orange solution. Once solvent was removed *in vacuo*, orange solids were collected and recrystallized from a concentrated MeCN solution, forming the MeCN-ligated CoPhNHC complex (**Figure 3.1b**). X-ray quality crystals were grown from slow diffusion of MeCN into a toluene solution of CoPhNHC . For simplicity, the molecular drawings of both compounds can be found in **Figure 3.1**.

Figure 3.1. Structure of CoSNHC (left) and CoPhNHC (right).



Electrochemical investigations of CoPhNHC showed 3 quasi-reversible oxidations at -0.362 V, 0.656 V, and 1.023 V versus Fc/Fc^+ in MeCN (**Figure 3.2**). Each oxidation formally represent the transformations from Co^{II} to Co^{III} , Co^{IV} , and Co^{V} .

Figure 3.2. Cyclic voltammogram of CoSNHC (red) compared to CoPhNHC (gold) in MeCN.

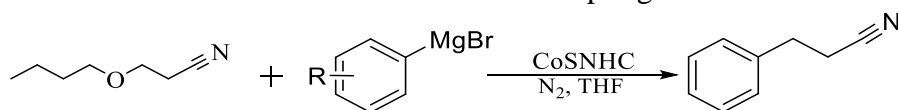


The UV-Vis spectrum of the complex shows only a single peak at 428 nm ($\epsilon = 1450 \text{ M}^{-1}, \text{ cm}^{-1}$). This spectrum is similar to that of CoSNHC, which has a peak at 430 nm ($\epsilon = 5300 \text{ M}^{-1}, \text{ cm}^{-1}$). Solution magnetic susceptibility measurements (Evans NMR method) analysis of CoPhNHC in CDCl_3 gives $\mu_{\text{eff}} = 2.38 \text{ } \mu\text{B}$, corresponding to a related spin value of $S=1/2$.

Ether C-O Bond Activation and Cross Coupling with Aryl Magnesium Halides

Previously work from our lab had found that CoSNHC is capable of activating the C-O bond in ether nitriles (cyanoalkyl ethers) and cross coupling the resulting nitrile fragment with aryl Grignards to generate aryl nitriles.⁹ A generic scheme is shown below in **Figure 3.3**.

Figure 3.3. Generic reaction scheme for C-O cross coupling reaction.

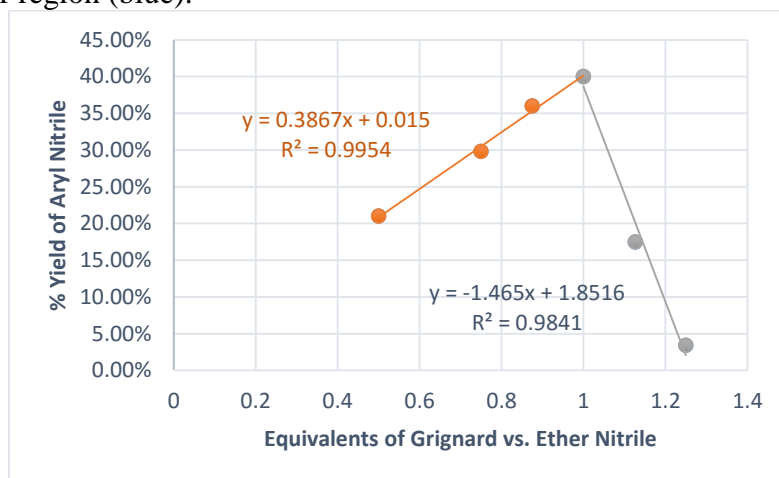


Optimization of Reaction Conditions

Optimization of the system was undertaken using 3-butoxypropionitrile (ether nitrile) and phenylmagnesium bromide (PhMgBr) as reagents with CoSNHC as the added catalyst. Initial reactions performed in THF at ambient temperature gave a yield of 41% with 1.65 mM of CoSNHC at 5% catalyst loading in THF after 24 hours. Under the same conditions, but using CoCl₂ in place of CoSNHC resulted in a yield of 12%. Combining the ether nitrile and PhMgBr without the presence of any cobalt does not result in any formation of product. Instead, the Grignard attacks the nitrile forming the expected imide salt and deprotonating unreacted ether nitrile, as evidenced by the ¹H NMR spectrum. Notably, treating this mixture with CoSNHC in conditions analogous to those described above also gives no product formation.

The concentrations of PhMgBr were varied to determine if the reaction could be driven with excess Grignard reagent. At constant CoSNHC concentrations with 20 equivalents of ether nitrile, PhMgBr was added in varying ratios, ranging from sub-stoichiometric to excess versus ether nitrile, corresponding to 0.5 to 1.5 equivalents. As shown in **Figure 3.4**, the resulting yields show a strongly linear correlation with equivalents of Grignard ranging from 0.5 to 1.0 equivalents (orange) whereas excess equivalents of Grignard greatly decrease the yield (grey) linearly. One equivalent of PhMgBr per ether nitrile was found to be optimal.

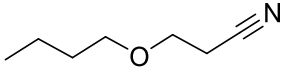
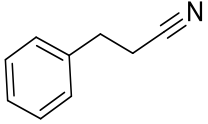
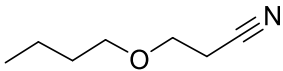
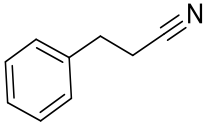
Figure 3.4. Varying Grignard equivalents versus ether nitrile with linear region (orange) and non-linear region (blue).



Based on the sharp decline of yields in the presence of excess PhMgBr, slow addition of Grignard was also explored as a way to reach a 1:1 ratio of PhMgBr to ether nitrile at 5% catalyst loading of CoSNHC. This was thought to avoid the potential deactivation pathway that occurs between the uncatalyzed reaction of PhMgBr with ether nitrile. Adding PhMgBr at a rate of 0.1 or 0.2 mmol/min resulted in yields of 22% and 26% respectively, just over half the yield of 41% obtained when PhMgBr is added immediately.

The reaction was then optimized for time under standard conditions, by quenching the reaction with excess methanol and determining the yield of the product after 5, 10, 30, and 60 minutes. The data were averaged across two runs with respective yields of 14.6%, 26.0%, 31.2%, and 40.8% respectively. In comparison to 41% over 24 h, the reaction was determined to have run to completion after 1 h. Added tetramethylethylenediamine (TMEDA), at one equivalent of TMEDA versus CoSNHC had no significant effect on yield, but 20 equivalents of TMEDA per CoSNHC caused a decrease in yield of nearly half to just 25% shown in **Table 3.1**.

Table 3.1. Impact of additives on C-C bond formation.

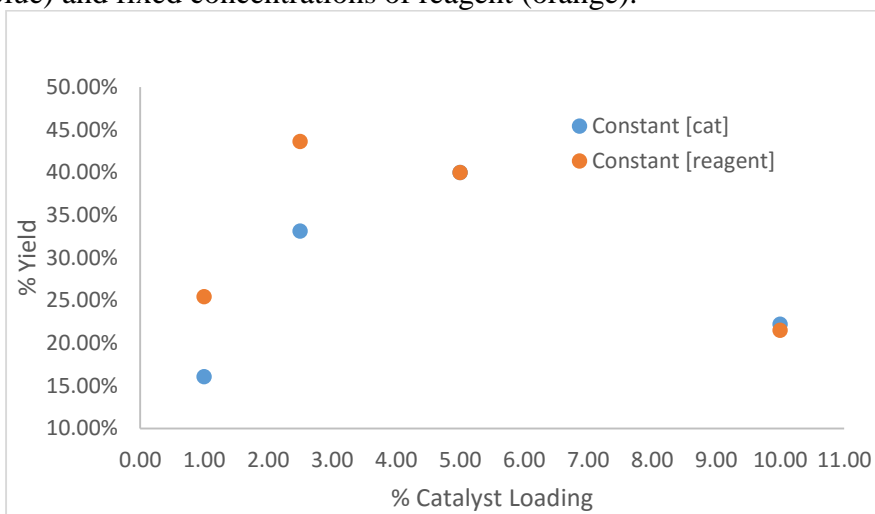
Reagent	Coupling Partner	Additive	Product	% Yield
	1 eq. PhMgBr	.05 eq. TMEDA		38%
	1 eq. PhMgBr	1 eq. TMEDA		25%

Finally, reactions were run under standard conditions with temperature varying from -40 °C, 20 °C, and 70 °C for 24 h resulting in respective yields of 28%, 41%, and 72%. This 72% yield at 70 °C is the highest yield achieved during optimization using CoSNHC.

Optimization of Reaction Concentrations and Catalyst Loading

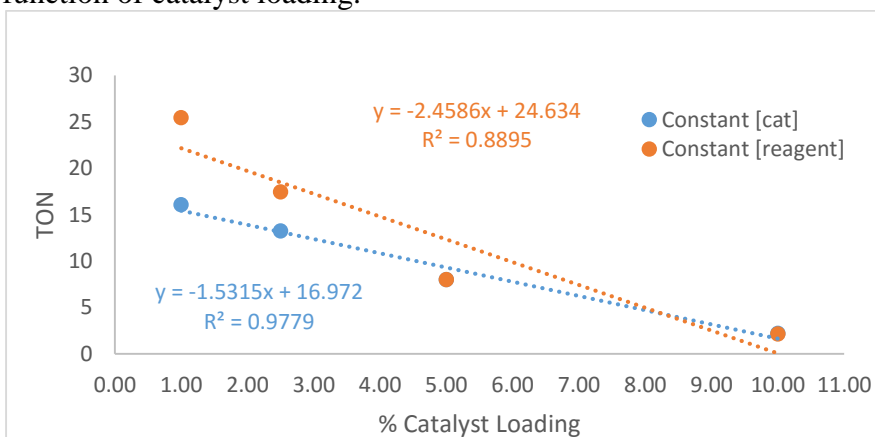
Optimal catalyst and substrate loadings were determined by varying both catalyst concentration and reagent concentrations in solution. First, the catalyst loading was varied between 1.0% and 10.0% by varying the substrate concentration from 16.5 to 165 mM at fixed [CoSNHC] = 1.65 mM. Next, catalyst loading was varied between 1.0% and 10.0% at fixed concentrations of substrate varying the concentration of CoSNHC from 3.3 mM to 0.33 mM. The results of these experiments are collected in **Figure 3.5**. The trends are non-linear. Yields peak at either 2.5% or 5.0% for constant [reagent] and constant [catalyst], respectively. In both cases, increased catalyst loading leads to pronounced decreases in the observed yields. A proposed rationale for this unexpected behavior is presented below.

Figure 3.5. Yields at various catalyst loadings of CoSNHC at fixed concentrations of catalyst (blue) and fixed concentrations of reagent (orange).



To assess efficiency of the individual catalyst molecule, it is better to compare the performance/efficiency of the catalyst at a given loading, shown as turnover numbers (TON). These data are shown in **Figure 3.6**.

Figure 3.6. Linearization of yields at various catalyst loadings of CoSNHC by measuring TON as a function of catalyst loading.



Under these conditions, the catalyst is most efficient at the lowest loading tested, 1.0 %. It is clear that keeping the concentration of reagent constant is most beneficial, as under these conditions at 1.0 % loading of CoSNHC has a TON of 25 while at constant concentration of CoSNHC a TON of only 16 was achieved.

Investigations into Substrate Tolerance

A variety of organic and organometallic molecules were explored as potential substrates for C-C cross coupling. Variations on 3-butoxypropionitrile included substrates with varying chain lengths between the butoxide fragment and the nitrile, such as 2-butoxyacetoneitrile, 4-butoxybutyronitrile, and 3-butoxybutyronitrile. The length of the butoxy fragment was also varied to include methoxy, ethoxy, and hydroxy substituent groups. The role of the nitrile as a directing group was also explored through variations of butoxy-ether linkage rigidity, other nitrogen and oxygen directing groups, and other potential metal- π bond substrates. Rigidity was explored at fixed chain length by using *o*-alkoxybenzotrile nitriles while primary and tertiary amines, alcohols, alkynes, and non-functionalized ethers were tested to determine any directing effect.

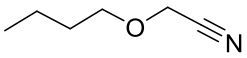
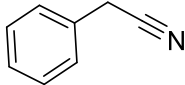
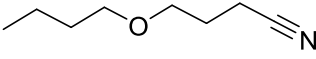
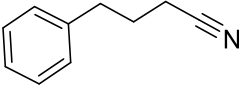
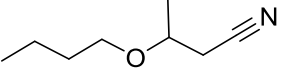
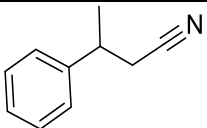
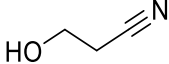
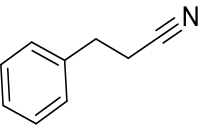
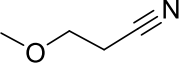
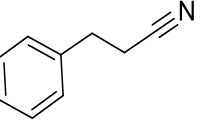
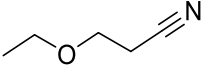
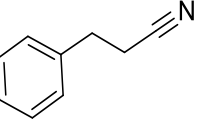
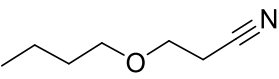
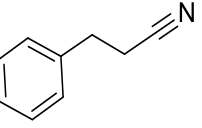
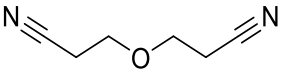
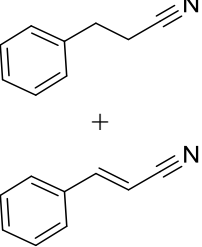
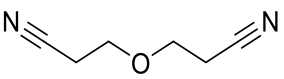
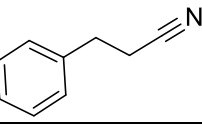
Kumada coupling was also explored using bromoacetoneitrile, chloroacetoneitrile, and 3-bromopropionitrile as analogues for 3-butoxypropionitrile. Substitutes for the organometallic determined reactivity with aryl lithiums, alkyl lithiums, alkyl Grignards, substituted aryl Grignards, and arylzinc reagents. Substituted aryl Grignards were used to determine functional tolerance, as well as assess the impact of steric bulk around the Grignard, and the potential for interactions with undirected aryl C-O substituent groups. In all cases, homocoupling and expected products were quantified via GC-MS.

Variation of C-O Substrates

First, the chain length between the butoxy and nitrile fragment was varied along with the length of the butoxy fragment to understand if either played any role in catalysis. All reactions were performed at ambient temperature for 24 h with 5% CoSNHC at 1.65 mM in THF. Phenylmagnesium bromide was used as the coupling partner. The results in

Table 3.2, show that the optimal linker between butoxy and nitrile is three carbons and that shorter alkoxy chains afford higher yields. Replacement of the alkoxy chain with a hydroxyl group resulted in no product formation. Consistent with Grignard reactions with protic reagents, large quantities of salt precipitated from the solution. Finally, a di-substituted ether, 2-cyanoethyl ether, was also tested using one and two equivalents of PhMgBr, one for each nitrile arm. When one equivalent of Grignard was used, cinnamitrile was seen for the first time in 4.5% yield, while the expected product formed in a slightly lower than expected 33.7% yield. If instead two equivalents of Grignard was added, the expected product is formed in 59.7% versus one starting equivalent of the 2-cyanoethyl ether. Side reactions were found to proceed with 4-butoxybutyronitrile and 3-butoxybutyronitrile, indicating minor products such as homocoupled nitrile fragments.

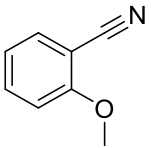
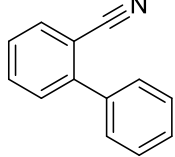
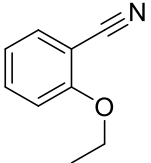
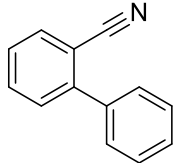
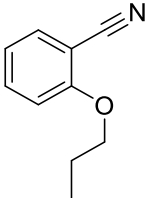
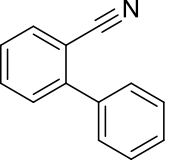
Table 3.2. Impact of varying butoxy-nitrile carbon linkers and alkoxy chain length on coupling of ether nitriles with phenylmagnesium bromide using 5% CoSNHC.

Reagent	Nitrile Chain Length	Alkoxy Chain Length	Coupling Partner	Product	% Yield
	C2	C4	1 eq. PhMgBr		<5%
	C4	C4	1 eq. PhMgBr		12.9%
	<i>sec</i> -C4	C4	1 eq. PhMgBr		7.9%
	C3	C0	2 eq. PhMgBr		N.R.
	C3	C1	1 eq. PhMgBr		64.8%
	C3	C2	1 eq. PhMgBr		56.2%
	C3	C4	1 eq. PhMgBr		41.0%
	C3,C3	--	1 eq. PhMgBr		33.7% + 4.5%
	C3,C3	--	2 eq. PhMgBr		59.7%

A variety of *o*-alkoxybenzonitriles were studied to determine if there was a dependence on the rigidity of the carbon fragment connecting ether and nitrile functional

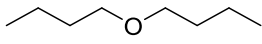
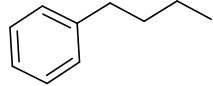
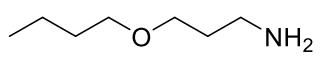
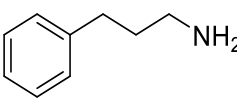
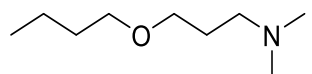
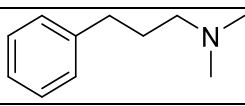
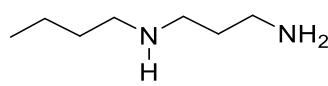
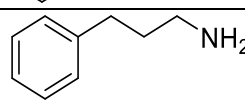
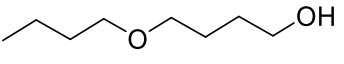
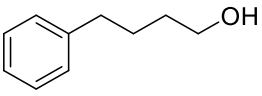
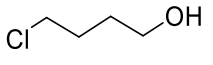
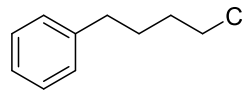
groups. Benzonitriles did not afford any of the expected C-C cross-coupling products by GC-MS analysis, as shown in **Table 3.3**.

Table 3.3. Impact of rigidity between alkoxy and nitrile chain, accounting for a variety of alkoxy chain lengths.

Reagent	Alkoxy Chain Length	Coupling Partner	Expected Product	% Yield
	C1	PhMgBr		N.R.
	C2	PhMgBr		N.R.
	C3	PhMgBr		N.R.

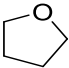
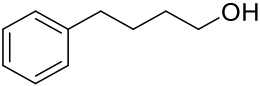
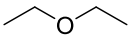
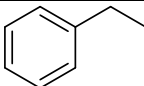
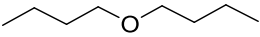
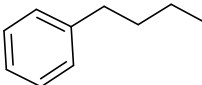
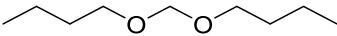
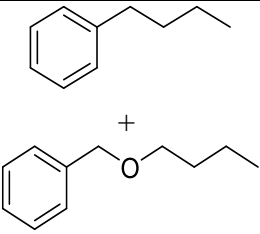
Ethers containing primary amines, tertiary amines, alcohols, and alkynes were tested for C-C cross coupling. Dibutyl ether, 3-butoxypropylamine and 3-butoxypropyl(dimethyl)amine were also tested which resulted in no product formation. Results are summarized below in **Table 3.4**. In each case, the only product formed was biphenyl, the product of PhMgBr homocoupling.

Table 3.4. Ability of other functional groups to drive for C-O activation, accounting for acidic proton quenching of Grignards.

Reagent	Equivalents of Grignard	Coupling Partner	Expected Product	% Yield
	1 eq.	PhMgBr		N.R.
	3 eq.	PhMgBr		N.R.
	1 eq.	PhMgBr		N.R.
	4 eq.	PhMgBr		N.R.
	2 eq.	PhMgBr		N.R.
	2 eq.	PhMgBr		N.R.

Finally, it should be noted THF and diethyl ether were unreactive ethers, as they were used as solvents. To confirm this, control reactions were performed with phenylmagnesium bromide as a coupling partner at 5% loading of CoSNHC at 1.65 mM unheated for 24 h. As shown below in **Table 3.5**, no coupling was observed for any substrate. In each case, no other product was found by GC-MS.

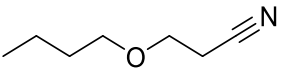
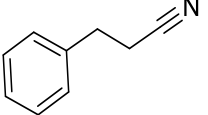
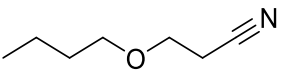
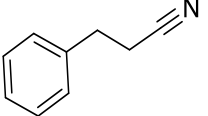
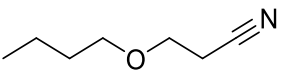
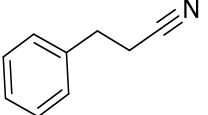
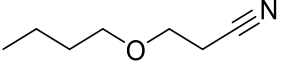
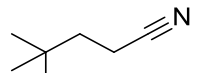
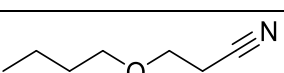
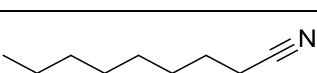
Table 3.5. Coupling of unactivated and undirected sp^3 C-O bonds with phenylmagnesium bromide at 5% CoSNHC. Etheric reagents are in large excess.

Reagent	Coupling Partner	Expected Product	% Yield
	PhMgBr		N.R.
	PhMgBr		N.R.
	PhMgBr		N.R.
	PhMgBr		N.R.

Variation of Organometallic Substrates

Aryl-lithium, aryl Grignard, and arylzinc reagents were explored to determine if a strong nucleophile was necessary for catalysis, or if a reagent more tolerant of nitriles would result in higher yields. Alkyl-lithium and alkyl Grignard reagents were also explored, to expand the scope of potential products. Reactions were completed using 3-butoxypropionitrile as the C-O reagent with 5% loading of CoSNHC at 1.65 mM concentration at ambient temperature for 24 h and then quenched by addition of MeOH. The results are summarized below in **Table 3.6**. Reactions using aryl organometallics produced biphenyl as a homocoupled product, while alkyl-lithium produced a homocoupled product.

Table 3.6. Coupling of 3-butoxypropionitrile with various organometallics at 5% CoSNHC at room temperature for 24 hours.

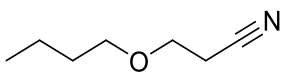
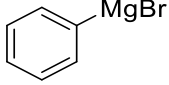
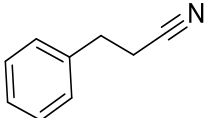
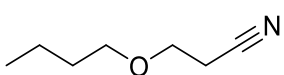
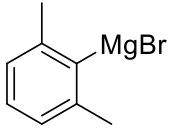
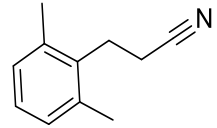
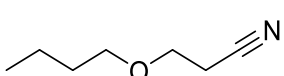
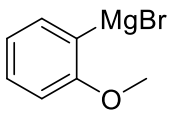
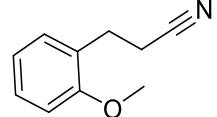

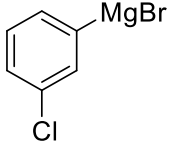
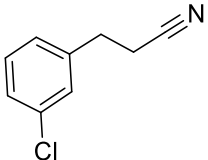
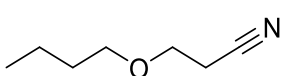
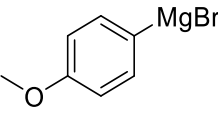
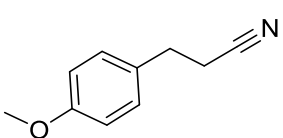
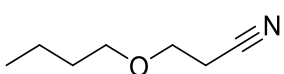
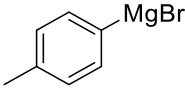
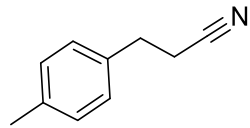
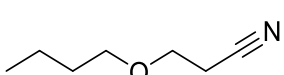
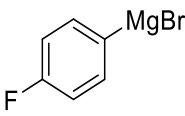
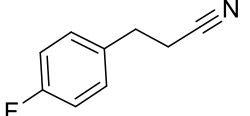
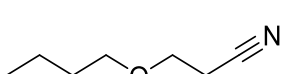
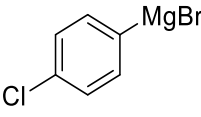
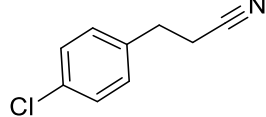
Reagent	Organometallic	Expected Product	% Yield
	PhLi		N.R.
	PhMgBr		41.0 %
	PhZnBr		N.R.
	<i>t</i> Bu-Li		<10%
	Hexyl-MgBr		N.R.

Phenylzinc bromide and phenyllithium were unable to couple via C-O bond cleavage, but *tert*-butyl lithium gave low yields (<10%) of the expected cross coupling product amid a slew of unidentified side products.

A variety of functional groups on the aryl ring were tested to determine their effects on catalysis. These reactions were run at 2.5% loading of CoSNHC at 0.825 mM and were heated to 70 °C for 1 hour using 3-butoxypropionitrile as a coupling partner. No side products were formed besides various substituted biphenyls. Due to the lack of commercially available products, products were quantified by consumption of ether. The validity of this approach was shown via a sample reaction using phenylmagnesium bromide as a coupling partner that found the cross coupling product and the unreacted ether nitrile summed to ~100% of the total ether nitrile reactant in the catalytic mixture. As collected in **Table 3.7**, the reaction is tolerant of fluoro- and chloro- functionalities as

well as aryl ethers. The reaction was also able to proceed in the presence of large steric bulk about the Grignard site, evidenced by 2,6-dimethylphenylmagnesium bromide having a yield of 31%. Interestingly, non-functionalized phenylmagnesium bromide performed the best under these conditions, with yields of 56%.

Table 3.7. Effect of various functional groups on the aryl ring of Grignards for coupling with 3-butoxypropionitrile. Yields are based on quantification of ether nitrile consumption.

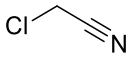
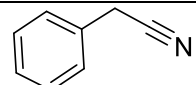
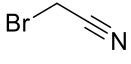
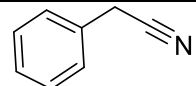
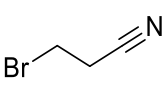
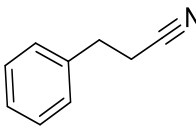
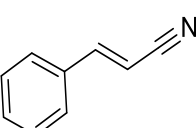
Reagent	Coupling Partner	Expected Product	% Yield
			55.8%
			31.3%
			25.0%
			12.5%
			45.0%
			23.1%
			28.4%
			23.0%

Kumada Coupling

To assess the importance of the alkoxide leaving group, a variety of halogen-containing alkyl nitriles were investigated for similar reactivity. Both chloroacetonitrile and bromoacetonitrile were examined to determine if there was any impact of the halogen

used while 3-bromopropionitrile was used to model 3-butoxypropionitrile. Reactions of these substrates with phenylmagnesium bromide were undertaken at 2.5% loading and heated to 70 °C for 1 h. The results are summarized in **Table 3.8**. In the case of 3-bromopropionitrile, the expected product was formed in much lower yields, just 9%, while the unsaturated product, was also formed in less than 1%. This side product does not form when 3-butoxypropionitrile is used as the coupling reagent.

Table 3.8. Kumada coupling of halogen-containing alkyl nitriles with PhMgBr with 2.5% CoSNHC under heated conditions for 1 hour.

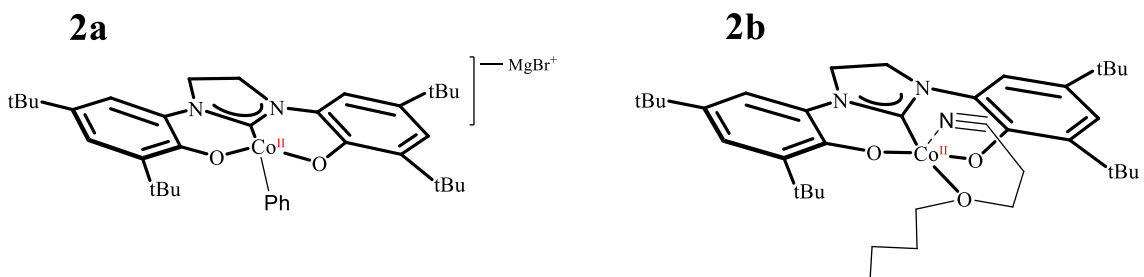
Reagent	Coupling Partner	Products	% Yield
	PhMgBr		4.1 %
	PhMgBr		< 1.0%
	PhMgBr	 + 	11.4% + <5.0%

It is important to note that halogen-containing alkyl nitriles react slowly with CoSNHC overtime, apparently producing an oxidative addition product. This contrasts with the 3-butoxypropionitrile, which is unreactive with CoSNHC in the absence of PhMgBr. Attempts to isolate the oxidative addition product of 3-bromopropionitrile to CoSNHC were unsuccessful due to decomposition of the complex to CoBr₂ as evidenced by UV-Vis.

Investigations into Catalytic Intermediate Species

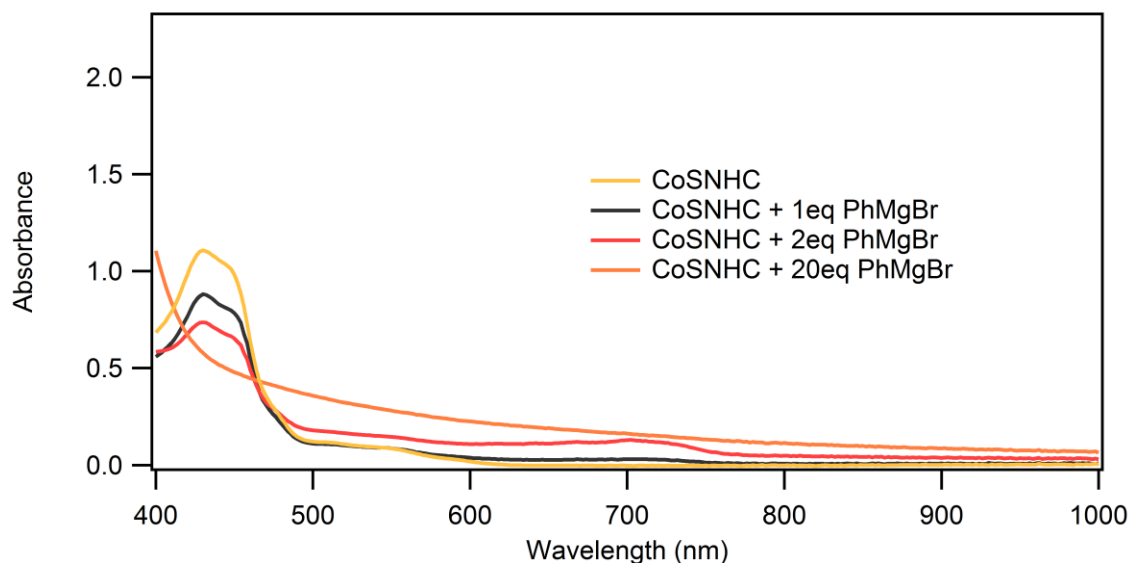
The catalyst was investigated for interactions with phenylmagnesium bromide and 3-butoxypropionitrile, giving rise to complexes **2a** (left) and **2b** (right) respectively as shown in **Figure 3.7**.

Figure 3.7. Proposed interactions of CoSNHC with reagents.



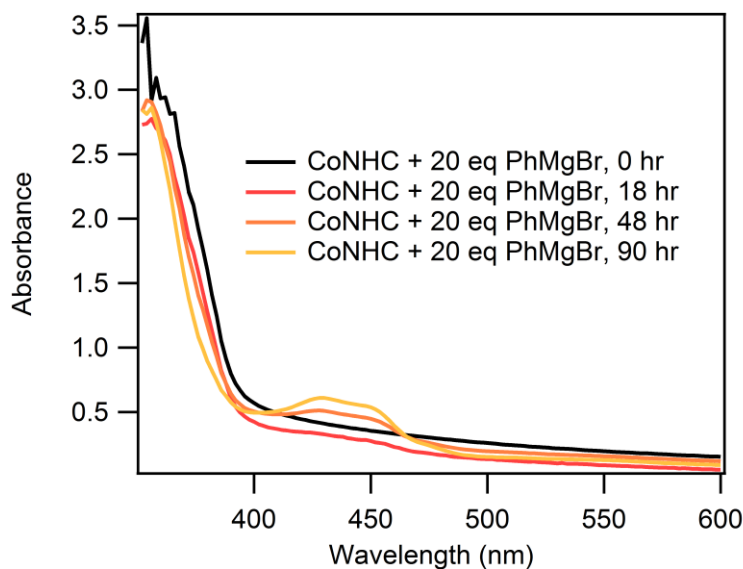
Compound **2a** is the product of transarylation to the metal with an outer sphere MgBr^+ counter ion, or transmetalation to the Co metal center with the loss of a Co-aryloxy bond. **2a** was first evidenced by attempts to determine if the catalyst was capable of solely homocoupling aryl Grignards to biphenyl. However, adding Grignard in a 1:1 ratio with CoSNHC only resulted in <5% formation of biphenyl. Similarly, if Grignard was added in excess in 1:2 or 1:4 ratios, the yield of biphenyl remains less than 8%. During these investigations, as higher ratios of Grignard were added to solutions of CoSNHC, the reaction mixture shifted from orange to black. This transformation was followed by UV-Vis spectrometry, using samples in cuvettes sealed under N_2 , and is shown below in **Figure 3.8** Subsequent additions of Grignard caused the known peak for CoSNHC at 430 nm in THF to disappear, forming a featureless spectra as the orange solution turned black. The featureless spectrum was assigned to intermediate species **2a**.

Figure 3.8. Bleaching of CoSNHC spectra with subsequent additions of Grignard.



Under catalytic conditions using 20 equivalents of Grignard, the spectrum assumes the shape of the orange line in **Figure 3.8**. If left for over 90 hours in the sealed cuvette the spectra will return to the expected shape of CoSNHC, reforming **1** at greater than 90% conversion as shown below in **Figure 3.9**. Alternatively, the process can be accelerated by addition of MeOH.

Figure 3.9. Reformation of CoSNHC from **2a** in a cuvette under sealed N₂ atmosphere.



Attempts to isolate a Grignard adduct were unsuccessful, largely due to the formation of **2a** requiring excess equivalents. However, a similar species, **2c**, could be formed using just one equivalent of phenyllithium, and this was studied as an analogous compound. The phenyllithium adduct species behaved differently by UV-Vis and was not reversible as found by UV-Vis spectrum in MeOH. **2c** could be isolated as a black solid. Addition of excess 3-butoxypropionitrile to **2c** in THF resulted in no product formation. Addition of two equivalents of PhLi to form **2c** resulted in 0.5 equivalents of biphenyl being produced, and a resulting black solution. Using this Co solution as a catalytic mixture with 20 equivalents of PhMgBr and 3-methoxypropionitrile results in only 14% conversion of product, roughly 1/5 of the expected yield and comparable to CoCl₂.

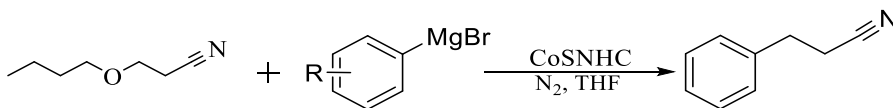
Another potential starting point in both catalytic cycles is the binding of 3-butoxypropionitrile to CoSNHC resulting in the formation of **2b**. **2b** was able to be synthesized a variety of ways, including dissolving CoSNHC in the minimal amount of neat 3-butoxypropionitrile yielding a red solution as well as by dissolving CoSNHC in benzene forming a green-brown solution and adding an excess of 3-butoxypropionitrile until a red solution forms. Isolation of **2b** from either synthesis by drying solvents resulted in a red solid that could be taken up in MeOH and examined via ESI to confirm the presence of **2b**.

DISCUSSION

The results presented herein are a novel example of sp^3 C-O bond activation for C-C bond formation. To the best of our knowledge, there are no other couplings of ether nitriles with substituted aryl Grignards. Optimization of the reaction found that the reaction proceed best when heated mildly, resulting in yields of 72% using CoSNHC as the catalyst at 5.0% loading. The reaction only occurs with nitrile functional groups, suggesting the role of the nitrile might be as a directing ligand, as discussed below. The reaction is tolerant of halogen-containing and aryl ether-containing Grignards.

Investigating Reaction Conditions of C-O Activation

Figure 4.1. Generic reaction scheme for C-O cross coupling reaction.



Interestingly, when optimized for ratios of PhMgBr to ether nitrile (**Figure 3.4**) there is a strongly linear trend from 0.5 to 1.0 equivalents, however it sharply decreases when excess Grignard is added such as 1.1 and 1.25 equivalents. This stands in sharp contrast, as it implies that Grignard is needed to activate the ether nitrile or catalyst in some fashion, while in excess it actually suppresses the reaction with the resulting inactive species showing no ability to participate in formation of the aryl nitrile product.

The addition of additives was also explored, as the idea of Grignard activation is not uncommon for C-O activation, however the addition of MgBr₂ to act as a Lewis Acid activator had no effect on yield.^{7,9} Similarly, additions of TMEDA, a known activator in

iron Kumada couplings, had no effect on yield at low equivalents or decreased overall yield when added in excess.

In an attempt to shift the formation of inactive species, Grignard was added slowly, however this was only found to reduce yields by approximately 50%. This means that the inactivation of either ether nitrile or catalyst is relatively fast and competes directly with productive formation of the aryl nitrile product. This equilibrium can be perturbed by the thermodynamics of the system, as temperature is shown to have a profound effect on reaction yields. Temperature optimization studies found the yield diminished by 30% when the reaction was run at -40 °C while nearly doubling from room temperature yields to 72% when run at 70 °C. It is also possible that temperature helps place a larger percentage of the catalyst in an active or excited state, thereby increasing yield.

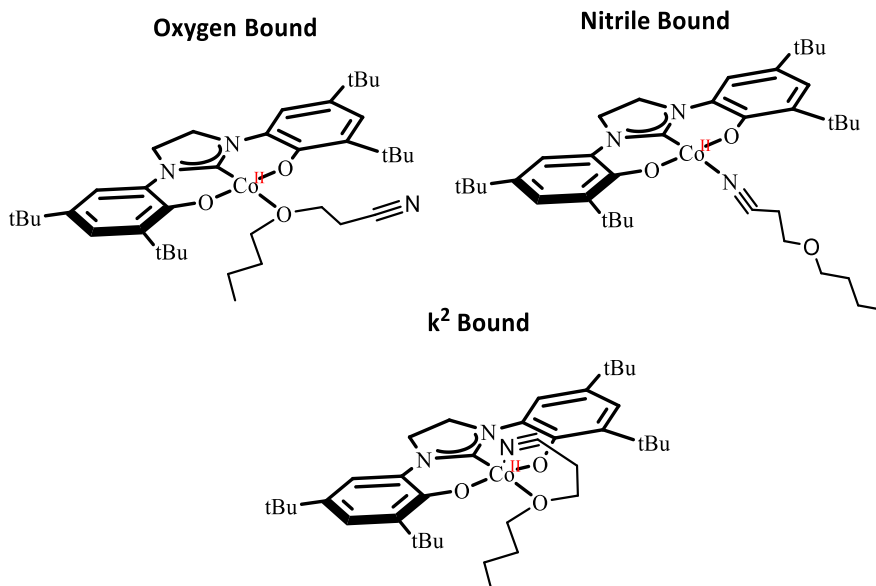
Due to the interplay of deactivation by Grignard versus catalysis, the reaction was also optimized for catalyst and reagent concentration as variations of catalyst loadings. What is interesting about these results, is that catalysts are generally viewed as having a set efficiency: a yield of 50% at 5% catalyst loading would imply near-quantitative yield at 10% loading. In this system, as shown in **Figure 3.5**, there seems to be a Goldilocks Effect, where the optimal yields are at 2.5% loading for constant [reagent] and 5.0% loading for constant [cat.]. Instead of increasing yields as loading increases, under both conditions, yields plummet at high catalyst loadings implicating the presence of a bimetallic deactivation pathway. This is further supported when the yields are linearized by conversion to TON in **Figure 3.6**, which clearly shows that as catalyst loadings

increase, catalyst efficiency decreases. This is consistent with bimetallic inactivation pathways.

Understanding Directing Group's Role in C-O Activation

Exploration of potential substrates found that undirected ethers, such as THF, diethyl ether, dibutyl ether, and dibutoxymethane were unreactive, while those with nitriles proceeded in low to moderate yields. Also the length of the carbon linker between ether and nitrile moiety played a large role in catalysis, as under screening conditions a two carbon linker had a yield of <5%, a three carbon linker had a yield of 40% and the four carbon linker had a yield of 13% (**Table 3.2**). This suggests that the role of the nitrile group might be as a directing ligand for C-O activation, and that the bite angle of the nitrile chain after C-O bond cleavage plays a role in catalysis. Possible configurations of this directing effect are shown in **Figure 4.2**.

Figure 4.2. Potential binding modes of 3-butoxypropionitrile to CoSNHC to form **2b**.



The importance of this binding was further explored by varying the rigidity of the three carbon linker by using *o*-alkoxybenzonitriles, which do not allow for any rotation in

the resulting nitrile fragment after cleavage. Surprisingly, none of these reagents gave the expected products suggesting that flexibility in the nitrile fragment is very important for catalysis (**Table 3.3**). It is also possible the system simply does not cleave sp^2 C-O bonds, though this is surprising because sp^2 C-O cleavage is generally viewed as easier and has multiple examples on both iron and nickel.^{7,11,15,17} To further account for this, 3-butoxybutyronitrile which has a methyl group installed next to the alkoxy chain was examined, as it introduced both steric bulk at the C-O cleaving site and slightly reduced flexibility. It also slightly deactivates the targeted C-O bond. The resulting coupled product was produced in only 8% yield, however it is difficult to determine which parameter caused this decrease.

Similar investigations into the length of the alkoxy chain testing methoxy, ethoxy, and butoxy propionitrile variants found it had an inverse effect on yield. With yields of 64.8%, 56.2%, and 41.0% respectively, it indicates that methoxy is the best leaving group for catalysis. This is not wholly unexpected, as investigations into reductions of dealkylation of bis(alkoxy)benzenes have long shown selectivity for shorter or longer alkoxy lengths depending on the dealkylating agent.²⁷ The exact cause of selectivity in this catalysis is not known in regards to a steric or electronic effect. The replacement of the alkoxy chain with a hydroxyl group was also investigated to determine if the ether moiety was necessary for catalysis to take place. The reaction did not proceed to form product, and even in the presence of two equivalents of Grignard to account for the acidic proton, only insoluble salts were formed.

Other directing groups such as amines and alcohols were also investigated, such as 3-butoxypropylamine or 4-butoxy-1-butanol, but these were found to be unreactive

even when accounting for the acidic protons (**Table 3.4**). This suggests that the reaction requires either a nitrile, tertiary amine, or a C-X multiple bond. Nitrogen directing groups were further explored by methylation of 3-butoxypropylamine forming the tertiary 3-butoxypropyl(dimethyl)amine, which resulted in no formation of product. Regardless, it is clear however that a directing group is necessary, as undirected sp^3 ethers such as dialkyl ethers were completely unreactive (**Table 3.5**).

Finally, a variety of organometallic coupling partners were explored including aryl and alkyl-lithium, aryl and alkyl Grignard, and arylzinc reagents in order of decreasing nucleophilicity. Tied to this nucleophilicity is the ability for the organometallic to readily attack nitriles and of those tested, only arylzinc reagents do not. Any reactivity at all is therefore unexpected, as it means the ether moiety has an inductively protecting effect on the nitrile. It is also interesting then that phenyllithium does not work as a coupling partner while *t*Bu-Li does and inversely, phenylmagnesium bromide does work as a coupling partner while hexylmagnesium bromide does not (**Table 3.6**). Phenylzinc bromide was also found to not be a viable coupling partner. Looking at the relative nucleophilicity of the coupling partners, these findings imply that the organometallic needs to strike a middle ground, as at both extremes neither phenyllithium nor phenylzinc bromide were viable coupling partners. This middle ground is nucleophilic enough to drive catalysis, while not being able to rapidly attack the nitrile moiety and stopping C-O activation. Though both aryl Grignard and alkyl-lithium reagents worked, *t*-BuLi formed a variety of side products implying some nucleophilic attack on the nitrile and was not explored further.

Since phenylmagnesium bromide reacted most cleanly with the highest yields, a variety of functionalized aryl Grignards were tested as coupling partners under optimized conditions (**Table 3.7**). As expected, the coupling was tolerant of fluoro- and chloro-groups as the complex is known to not readily undergo oxidative addition.⁶ Also, aryl methyl ether functional groups were tolerated, which had already been supported by lack of reactivity with *o*-alkoxybenzotriles. It is interesting that construction of a Hammett plot was not possible, as no general trend could be found however there was a tendency for higher yields to favor electron withdrawing species, with *p*-methoxy achieving the second highest yield of 45.0 %. Unexpectedly, the reaction was unhindered by steric bulk, such as by the use of 2,6-dimethylphenyl Grignard, which had the third highest yield of 31.3%.

Since the reaction readily proceeded with aryl Grignards, analogous Kumada coupling systems were explored. Previous investigations with CoSNHC found it sluggish or unable to oxidatively add aryl or alkyl halides. However, the inclusion of a nitrile directing group moiety was explored based on the strong dependence on its inclusion for C-O activation and for potential as a model system. Surprisingly, the nitrile was able to act as a directing group for the oxidative addition of these halogenic nitriles to CoSNHC, which was not possible with 3-butoxypropionitrile. This means that the model Kumada system undergoes a fundamentally different pathway. Regardless, halogenic nitriles were tested under optimal conditions for coupling with phenylmagnesium bromide resulting in poor yields. Use of acetonitrile derivatives yielded <5.0 % of the desired product and the halogenic analog for 3-butoxypropionitrile, 3-bromopropionitrile, was found to yield the

product in only 11.4 % yield and form a β -hydride elimination product in <5.0 % yield (**Table 3.8**).

Determining the Reaction Pathway of C-O Cleavage and C-C Formation

After exploring both the substrate scope and optimizing the reaction conditions, it is important to understand mechanistically what is occurring in solution. This knowledge ultimately allows for the design of better catalysts by stabilizing active catalytic species or disfavoring known off-cycle intermediates. Early mechanistic investigations focused on the CoSNHC catalyzed C-O coupling as a pseudo-Kumada reaction; however since the catalyst cannot oxidatively add the substrate without the presence of Grignard, the Kumada reaction proceeds through a fundamentally different mechanism. This is exemplified in results discussed above, which found that when bromide was substituted for the butoxide leaving group, the halogenic nitrile reacted with CoSNHC to form an oxidative adduct product. Further evidence for a difference in reactivity is when the bromo analogue is coupled with PhMgBr, the unsaturated product is present in small yields (**Table 3.8**). However, during C-O coupling, this species is never formed.

Due to the dependence on the presence of Grignard, a strong nucleophile and base, two potential catalytic cycles were proposed, either a redox-active pathway or a redox-inactive acid-base pathway. A radical pathway was not explored, as in all reactions run, expected radical by-products such as dialkyl nitriles, peroxides, or aryl butyl ethers are not formed. The acid-base pathway is shown in **Figure 4.3** and the redox-active pathway is shown in **Figure 4.4**.

Figure 4.3. Redox-neutral pathway of C-O activation via CoSNHC. The ligand arms have been excluded for simplicity and size.

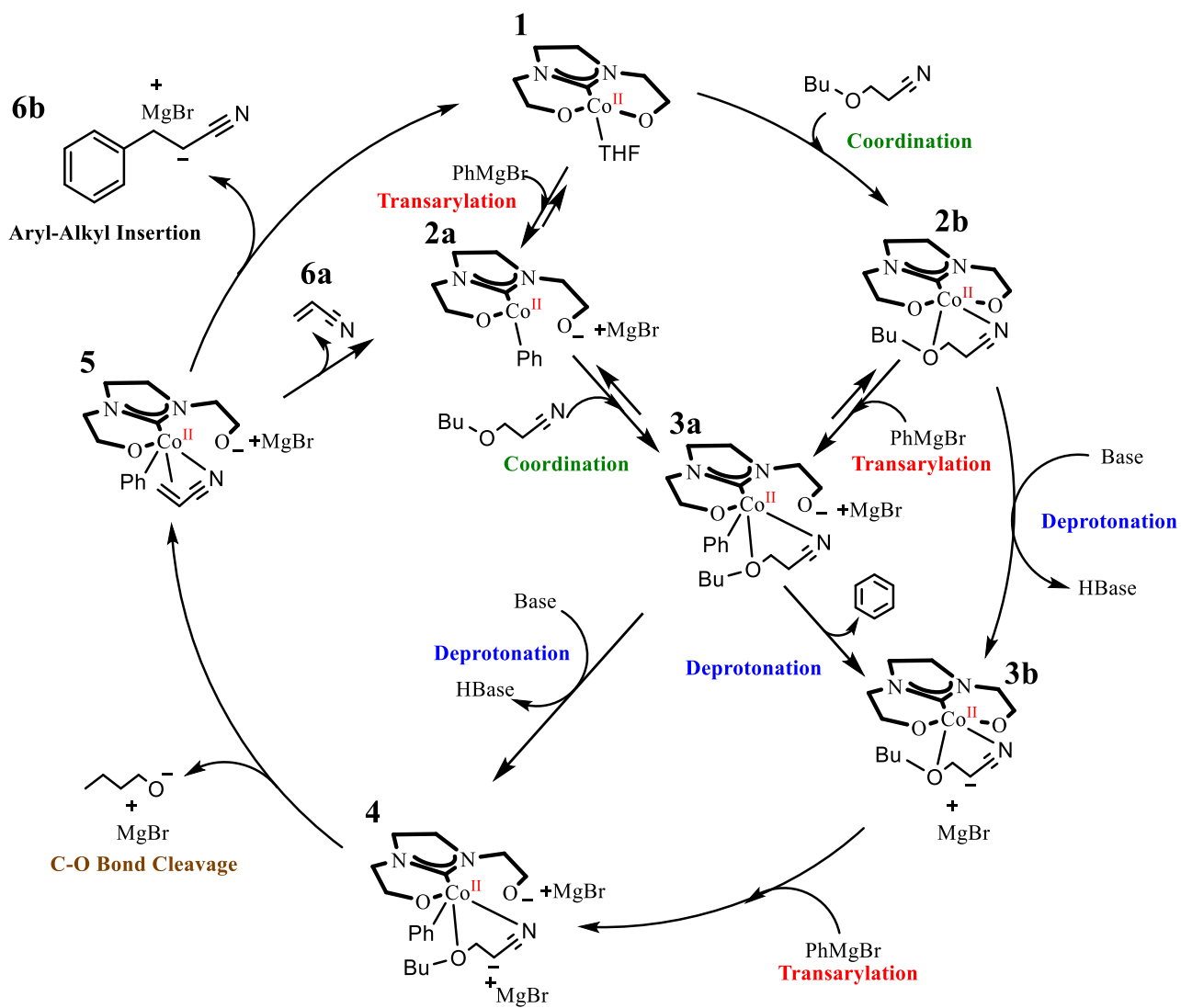
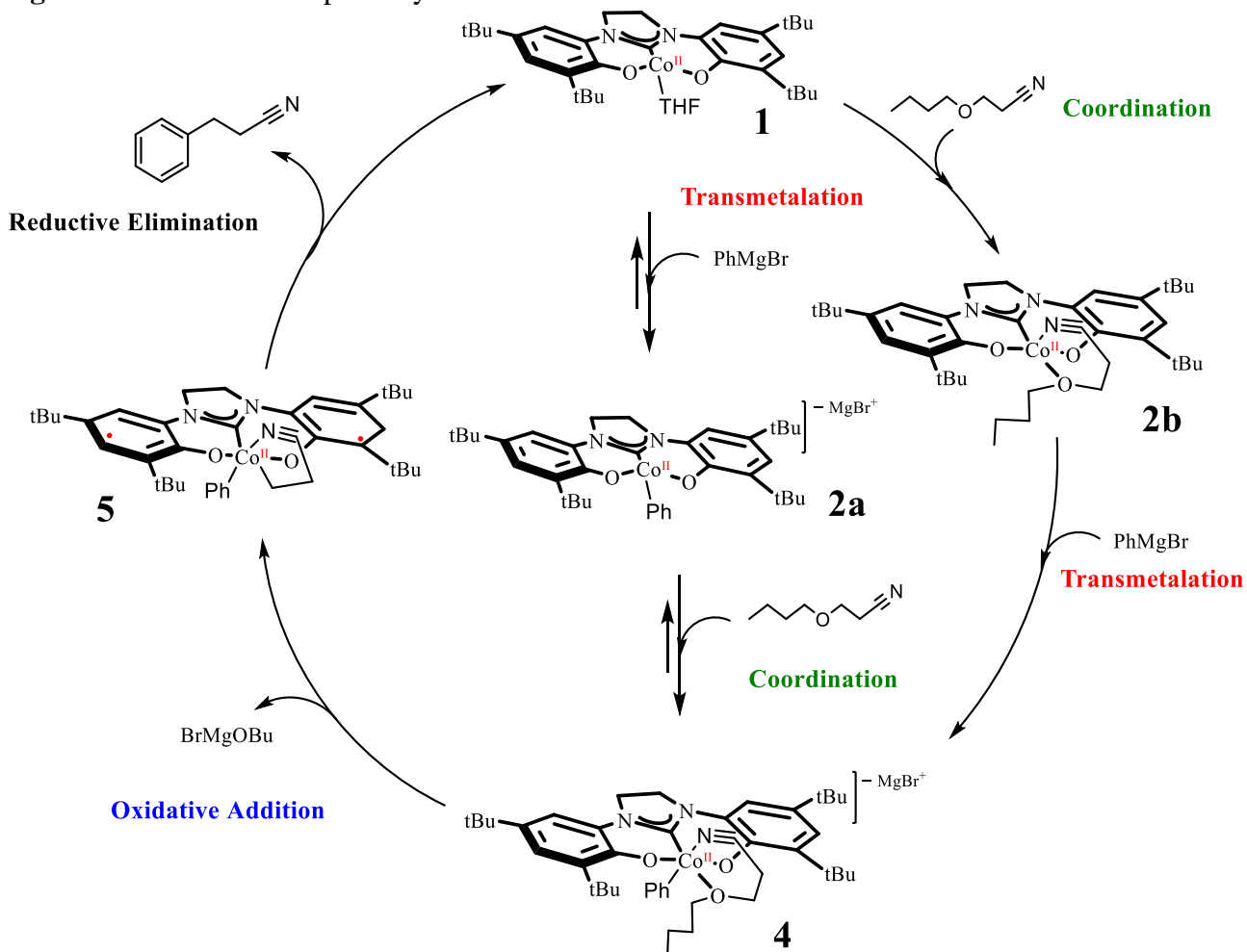


Figure 4.4. Redox-active pathway of C-O activation via CoSNHC.



Both cycles relied on two initial intermediates, **2a** and **2b**, formed as adducts of either PhMgBr or the ether nitrile respectively. **2a** was only possible in the presence of excess equivalents of Grignard, but was also synthesized with one and two equivalents of phenyllithium creating an analogous **2c**. **2a** was studied *in situ*, but was not isolated, by UV-Vis, which found the Grignard adduct was reversible in the presence of acidic protons or over time. **2b** was able to be isolated as a red solid and was studied in this state as a catalytic intermediate. For stoichiometric reactivity, **2c** was used instead of **2a**, as it could be isolated without the presence of excess organometallic. When **2c** was treated with excess ether nitrile no product formed, while reaction of **2b** with excess Grignard

did. However, use of **2c** as a catalytic solution resulted in a decreased yield of 14%. This is equivalent to the CoCl_2 control. This implies that **2c**, and by extension **2a**, are off-cycle intermediates that do not promote catalysis, and rationalizes why excess or higher concentrations of Grignard in solution decrease catalysis. It also means that **2b** is a viable intermediate in the catalytic pathway. Moving past both **2a** and **2b**, both cycles begin to diverge. Experimentally it is hard to prove the redox-active pathway, as the intermediate **4** is immediately reactive and leads to formation of product without any imagined side reactions. It is also difficult to study the reaction using NMR spectroscopy as the catalyst is paramagnetic. Further experimentation therefore focused on redox-neutral pathways and its intermediates.

Diving further into the redox-neutral pathway, the expected catalytic intermediately preceding C-O cleavage is **4**, which goes on to form **5**, a bound acrylonitrile species. **5** is also then immediately active to form one of two products: acrylonitrile (**6a**) or a deprotonated phenylpropionitrile (**6b**). Free acrylonitrile is not the known product of this reaction, however Grignards are known to perform 1,3-insertions into some unsaturated nitriles, which would result in **6b** *in situ*. To test this, acrylonitrile was substituted for 3-butoxypropionitrile and run under standard conditions, which resulted in no formation of the expected product. Similarly, a control reaction mixing acrylonitrile and phenylmagnesium bromide showed that the Grignard did not insert into the carbon-carbon double bond. **6b** looks similar to the product, however it is in its deprotonated state which is ultimately protonated by quenching with MeOH or by reacting with protonated bases *in situ*. Quenching a catalytic reaction between the ether nitrile and Grignard with CD_3OD did result in deuterium incorporation in the product.

Control reactions showed this was not mechanistically significant however, as stirring the phenylpropionitrile product in CD_3OD in the presence of catalyst also results in deuterium incorporation. Simply stirring phenylpropionitrile in CD_3OD does not result in deuterium incorporation.

CONCLUSIONS

Activations of C-O bonds are important because of their potential role in opening up new synthetic routes for fine chemicals, particularly through late-stage functionalization. However, past work on Co has only shown widespread reactivity with activated C-O bonds through sulfamate or carbamate coupling partners for carbon-carbon bond formation.^{7,12,13} Recent work has shown the ability to activate both aryl and benzylic ethers, however until this work no purely sp³ ether had been activated for C-C bond formation.^{7,10-13,16-18} The work presented in this thesis shows that tridentate cobalt bisphenoxide NHC catalysts are capable of coupling ether nitriles with aryl Grignards, where the nitrile moiety acts as a direction group for C-O bond cleavage. The reaction was shown to proceed in moderate yields under heated conditions, achieving yields of 72% at 5% of CoSNHC when heated to 70 °C. Further investigations into substrate scope found the catalyst was unable to activate undirected C-O bonds, and that the length of the nitrile chain played a large role in catalysis. The chain could not be too rigid, as this slowed catalysis in the case of 3-butoxy-butyronitrile and shutdown catalysis when *o*-alkoxybenzonnitriles were used. It is important to note in the later case this is a sp² C-O bond, which is different than an sp³ but has seen wider success in functionalization.^{7,11,15,17} Investigations into functional group tolerance of Grignards showed the reaction was tolerant of halogens and aryl ethers and tolerated large steric bulk about the Grignard as demonstrated by 2,6-dimethylphenylmagnesium bromide.

Mechanistic investigations into the catalytic pathway ruled out a radical pathway based on the lack of any radical-based products. A redox-neutral acid-base pathway

based on deprotonation of the ether nitrile was then explored. This deprotonated species was shown to not be active and extensive investigations into acrylonitrile as a reagent intermediate were unsuccessful in forming any product. Base-catalyzed reactivity was also investigated and was also found to be unsuccessful in forming product. A mixed redox-active base-catalyzed pathway is also ruled out because the deprotonated ether nitrile is incapable of forming the product under catalytic conditions.

FUTURE WORK

Given the clear focus on both reaction optimization of conditions and substrates as well as mechanistic understanding, it will be important to better characterize early catalytic intermediates and understand what features drive catalysis outside of directing groups. This will allow for improved catalyst design and generalize the coupling to undirected sp^3 C-O bonds.

To better understand the early catalytic intermediates **2a** and **2b**, X-ray diffraction-quality crystals would need to be grown to allow for crystallographic study and determination of the solid-state structure. In the case of **2a**, this would allow better understanding of how the Grignard adduct is stabilized while for **2b**, it would determine the binding mode of the ether nitrile. Understanding the binding mode will indicate at what position the C-O bond is cleaved, and allow improved catalyst design to favor this binding mode.

The knowledge gained from **2a** would allow improved design to disfavor this deactivating pathway while knowledge of **2b** would allow improved design focused on stabilizing the favored binding mode of the C-O bond, improving catalysis. One example would be if **2b** is found to favor the C-O bond to be *cis* to the carbene. By modifying the backbone of the carbene or the linking moiety, it would be possible to drive the C-O reagents into the axial position, and may then not even require a directing group.

Ultimately, after designing better catalysts it is important to generalize the reaction to undirected bonds, as this would allow for the functionalization of easily

accessible compounds such as diethyl ether, or for the late-stage functionalization of fine chemicals.

REFERENCES

- (1) Roughley, S. D.; Jordan, A. M. *Journal of Medicinal Chemistry* **2011**, *54*, 3451.
- (2) Chirik, P. J., E; Bedford, R; DeBeer, S; Fandrick, D; Garg, N; Hammes-Schiffer, S; Hanson, S; Holland, P; Ladipo, F; Weller, K; Montgomery, J; Morris, R; Stahl, S; Tedrow, J; Tilley, T. D; Tudge, M; Weix, D; Zubris, D; Bessel, C; Ren, T; **2013**, 23.
- (3) Su, B.; Cao, Z.-C.; Shi, Z.-J. *Accounts of Chemical Research* **2015**.
- (4) Sherry, B. D.; Fürstner, A. *Accounts of Chemical Research* **2008**, *41*, 1500.
- (5) Bedford, R. B. *Accounts of Chemical Research* **2015**, *48*, 1485.
- (6) Bayless, M. B.; Harris, C. F.; Bruch, Q. J.; Soper, J. D. *Manuscript in preparation*. 2016.
- (7) Su, B.; Cao, Z.-C.; Shi, Z.-J. *Accounts of Chemical Research* **2015**, *48*, 886.
- (8) Bauer, G.; Wodrich, M. D.; Scopelliti, R.; Hu, X. *Organometallics* **2015**, *34*, 289.
- (9) Bruch, Q. J.; Bayless, M. B.; Soper, J. D. *Manuscript in preparation*. 2016.
- (10) Cornella, J.; Gómez-Bengoa, E.; Martin, R. *Journal of the American Chemical Society* **2013**, *135*, 1997.
- (11) Cornella, J.; Zarate, C.; Martin, R. *Chemical Society Reviews* **2014**, *43*, 8081.
- (12) Song, W.; Ackermann, L. *Angewandte Chemie International Edition* **2012**, *51*, 8251.
- (13) Yu, D.-G.; Wang, X.; Zhu, R.-Y.; Luo, S.; Zhang, X.-B.; Wang, B.-Q.; Wang, L.; Shi, Z.-J. *Journal of the American Chemical Society* **2012**, *134*, 14638.
- (14) Amatore, M.; Gosmini, C.; Périchon, J. *European Journal of Organic Chemistry* **2005**, *2005*, 989.
- (15) Tasker, S. Z.; Standley, E. A.; Jamison, T. F. *Nature* **2014**, *509*, 299.
- (16) Yoshikai, N.; Mashima, H.; Nakamura, E. *Journal of the American Chemical Society* **2005**, *127*, 17978.
- (17) Tobisu, M.; Chatani, N. *Accounts of Chemical Research* **2015**, *48*, 1717.
- (18) Luo, S.; Yu, D.-G.; Zhu, R.-Y.; Wang, X.; Wang, L.; Shi, Z.-J. *Chemical Communications* **2013**, *49*, 7794.
- (19) Palmer, W. N.; Diao, T.; Pappas, I.; Chirik, P. J. *ACS Catalysis* **2015**, *5*, 622.
- (20) Smith, A. L.; Hardcastle, K. I.; Soper, J. D. *Journal of the American Chemical Society* **2010**, *132*, 14358.
- (21) Smith, A. L.; Clapp, L. A.; Hardcastle, K. I.; Soper, J. D. *Polyhedron* **2010**, *29*, 164.
- (22) Borré, E.; Dahm, G.; Aliprandi, A.; Mauro, M.; Dagorne, S.; Bellemin-Lapponnaz, S. *Organometallics* **2014**, *33*, 4374.
- (23) Romain, C.; Miqueu, K.; Sotiropoulos, J.-M.; Bellemin-Lapponnaz, S.; Dagorne, S. *Angewandte Chemie International Edition* **2010**, *49*, 2198.
- (24) Romain, C.; Fliedel, C.; Bellemin-Lapponnaz, S.; Dagorne, S. *Organometallics* **2014**, *33*, 5730.
- (25) Evans, D. F. *Journal of the Chemical Society (Resumed)* **1959**, 2003.
- (26) Live, D. H.; Chan, S. I. *Analytical Chemistry* **1970**, *42*, 791.
- (27) Testaferri, L.; Tiecco, M.; Tingoli, M.; Chianelli, D.; Montanucci, M. *Tetrahedron* **1982**, *38*, 3687.